

Article

Cold-Water Corals in Gas Hydrate Drilling Cores from the South China Sea: Occurrences, Geochemical Characteristics and Their Relationship to Methane Seepages

Yinan Deng ^{1,2,3,†} , Fang Chen ^{1,3,*}, Niu Li ^{3,4,5,*†}, Meng Jin ^{4,6}, Jun Cao ^{1,3}, Hong Chen ¹, Yang Zhou ¹, Cong Wu ¹, Chang Zhuang ¹, Yi Zhao ¹ and Sihai Cheng ¹

¹ MNR Key Laboratory of Marine Mineral Resources, Guangzhou Marine Geological Survey, Guangzhou 510075, China; dengyinan@126.com (Y.D.); caojun_031051@126.com (J.C.); chenhong@gmgs.cn (H.C.); zhouyang@gmgs.cn (Y.Z.); gzdiatom@163.com (C.W.); zhchdatou@126.com (C.Z.); liniu@mail.sysu.edu.cn (Y.Z.); chengsihai@163.com (S.C.)

² Research Center for Earth System Science, Yunnan University, Kunming 650091, China

³ Southern Marine Science and Engineering Guangdong Laboratory (Guangzhou), Guangzhou 511458, China

⁴ CAS Key Laboratory of Ocean and Marginal Sea Geology, South China Sea Institute of Oceanology, Chinese Academy of Sciences, Guangzhou 510301, China; jinmeng@scsio.ac.cn

⁵ Innovation Academy of South China Sea Ecology and Environmental Engineering, Chinese Academy of Sciences Guangzhou, Guangzhou 510301, China

⁶ University of Chinese Academy of Sciences, Beijing 100049, China

* Correspondence: Zhchenfang66@21cn.com (F.C.); liniu@scsio.ac.cn (N.L.)

† Both authors should be regarded as joint first authors.

Received: 1 November 2019; Accepted: 27 November 2019; Published: 29 November 2019



Abstract: Cold-water corals (CWCs) are frequently found at cold seep areas. However, the relationship between fluid seepage and CWC development is not clear. Here, for the first time, we report the occurrences, species identification, mineralogy, carbon and oxygen isotopes, as well as elemental compositions of fossil CWC skeletons from gas-hydrate-bearing sediment in drilling cores from the South China Sea (SCS). Three sites (GMGS-08, GMGS-09B, and GMGS-16) were investigated but CWCs were only found at one site (GMGS-09B). Interestingly, the CWCs were found in three horizons and they were all embedded with authigenic carbonates. Three genera of fossil CWCs (*Crispatotrochus* sp., *Solenosmilium* sp. and *Enallopsammia* sp.) were identified. The CWC fragments are predominantly aragonite. The CWCs exhibit $\delta^{13}\text{C}$ values between -8.4‰ and -0.6‰ that are significantly higher than $\delta^{13}\text{C}$ values of the associated seep carbonates ($\delta^{13}\text{C}$ values with an average of -55.6‰ , $n = 19$), which indicates a carbon source other than methane for the CWCs. It appears that authigenic carbonates provide a substratum for coral colonization. Bathymetric high points, appropriate water temperature and stronger bottom-water currents at site GMGS-09B might be crucial to keep conditions favorable for the growth of CWCs in the studied area. In addition, high trace-element concentrations of Cr, Ni, Pb, U, Ba, Th, and Sr suggest that the CWCs are influenced by strong fluid seepage that can reach the water-sediment interface, and associated microbial activity. Hence, it also becomes evident that CWCs in hydrocarbon-rich seepage areas not only provide a critical constraint on the impact of fluid emission on the bottom water chemistry, but also are likely to be very precise recorders of the end time of cold seep activity.

Keywords: cold water corals; methane seeps; carbon and oxygen isotope; authigenic carbonate; South China Sea

1. Introduction

Cold-water corals (CWCs), also termed deep-water corals, belong to the phylum Cnidaria. They include black corals (Antipatharia), stony corals (Scleractinia), hydrocorals (Stylasteridae), and soft corals (Octocorallia) [1,2]. These corals commonly occur in marine settings on continental margins, slopes, seamounts, and deep-sea basins in water depths of 30–1000 m, e.g., the moderately deep parts of the Southern Ocean and North Atlantic [3–5]. Rather than relying on symbiotic algae, the shallow-water coral's food supply, CWCs feed on plankton, organic matter, and tiny organisms in the oceans [1,6]. As such, CWCs are able to live in environments without sunlight and can provide paleoceanographic records in regions where other fossils are usually sparse [2].

Previous studies of CWCs have focused mainly on the geochemical record of deep-ocean changes archived in their skeletons [2,7]. Accurate dating by uranium-series disequilibrium and ^{14}C systems are facilitated by the high contents of U in their aragonitic skeletons [8–13]. Various geochemical proxies, including isotopes of carbon, oxygen, and neodymium, rare-earth elements (REEs), trace elements, and Ba/Ca, Mg/Ca and Sr/Ca ratios of CWC skeletons are commonly used to reveal oceanic processes such as carbon cycling [14,15], past water-mass changes [16–18], hydrothermal activity [7], changes in water temperature [19], and ocean acidification [20].

It has been proposed that the development of CWCs is controlled by various oceanographic conditions, including salinity, temperature, substrate, tractive current, and dissolved oxygen [21], as well as hydrocarbon seepage [22]. CWCs have been reported in association with hydrocarbon seeps in Norwegian fjords [6], offshore Ireland [23], the Kristen hydrocarbon field [24], the Norwegian Margin [25], the Hikurangi Margin (New Zealand) [26,27], eastern central Atlantic [28], the Gulf of Mexico [29], and the Gulf of Cádiz [30]. However, the influence of fluid seepage on CWC growth is not yet fully understood. One theory, termed the “hydraulic theory”, suggests that the energy and nutrient supply of CWCs may be directly fueled by cold seepage [22,31,32]. However, the absence of DNA from methane- and sulfide-oxidizing microbes in CWCs from an active hydrocarbon-rich seepage area of the Gulf of Cádiz indicates that CWCs do not harbor the chemosynthetic symbionts required to consume the reduced compounds in hydrocarbon-rich fluids [33]. It is possible that CWCs use authigenic carbonates, formed through anaerobic oxidation of methane (AOM) mediated by a syntrophic consortium of anaerobic methanotrophic archaea and sulfate-reducing bacteria [34–39], as a hard substrate for coral larval settlement [26,33,40–42]. In addition, CWCs potentially benefit from fluid-seepage-related structures such as mud volcanoes and carbonate mounds, as these structures provide morphological barriers that direct bottom currents to deliver nutrients to the corals [33,43,44].

CWCs in the South China Sea (SCS) were first discovered by Bassett-Smith [45] near the Zhongsha Islands and the Nansha Islands. Subsequently, many species of CWCs have been observed near the Xisha Islands and along the northern margin of the SCS [46]. Previous studies have focused mostly on species identification and ecological analysis with only limited reports of geochemical data. No evidence of CWCs being present in cold-seep areas of the SCS was reported until 2013, when abundant authigenic carbonates and cold-seep biota including CWCs were discovered in gas-hydrate-bearing sediments from cores GMGS2-08, GMGS2-09B, and GMGS2-16 obtained during China's second gas-hydrate drilling expedition (GMGS-2) (Figure 1). Despite the near-identical oceanographic and sedimentological conditions of the three drill cores, CWCs were found only at core site GMGS2-09B (Figure 2). However, the exact environmental conditions that regulate the occurrence of CWCs in this region remain unresolved. These gas-hydrate drill cores represent excellent materials to study the environmental factors that affect CWC development in methane-rich settings.

The present study reports, for the first time, species identification, mineralogy, and geochemistry (carbon and oxygen isotopes and major and trace elements) of three CWC species (*Crispatotrochus* sp., *Solenosmilia* sp., and *Enallopsammia* sp.) retrieved from core GMGS-2 from a cold-seep area in the SCS (Figure 2). Our results provide insights into the relationship between fluid seepage and CWC development. Furthermore, the investigation helps to improve understanding of the factors that

control coral growth and of interpretations of bottom-water chemistry recorded by CWC skeletons in fluid-seepage settings.

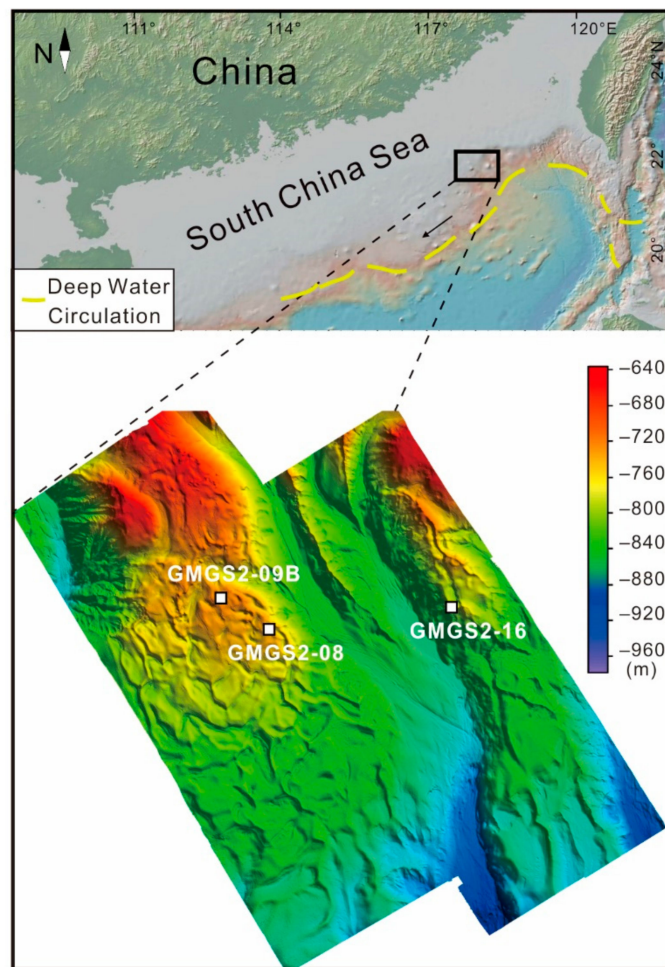


Figure 1. Location of sites GMGS2-08, GMGS2-09B, and GMGS2-16 on the northern continental slope of the South China Sea. Deep-water currents are after Liu et al. [47].

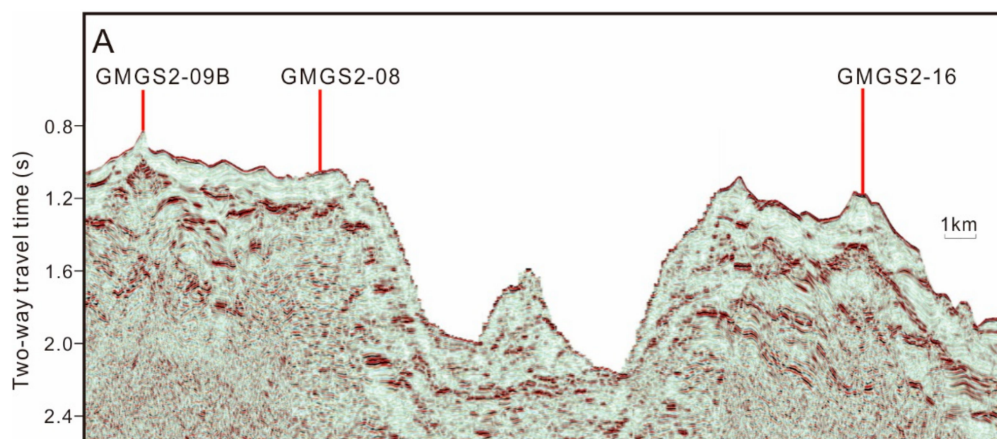


Figure 2. Cont.

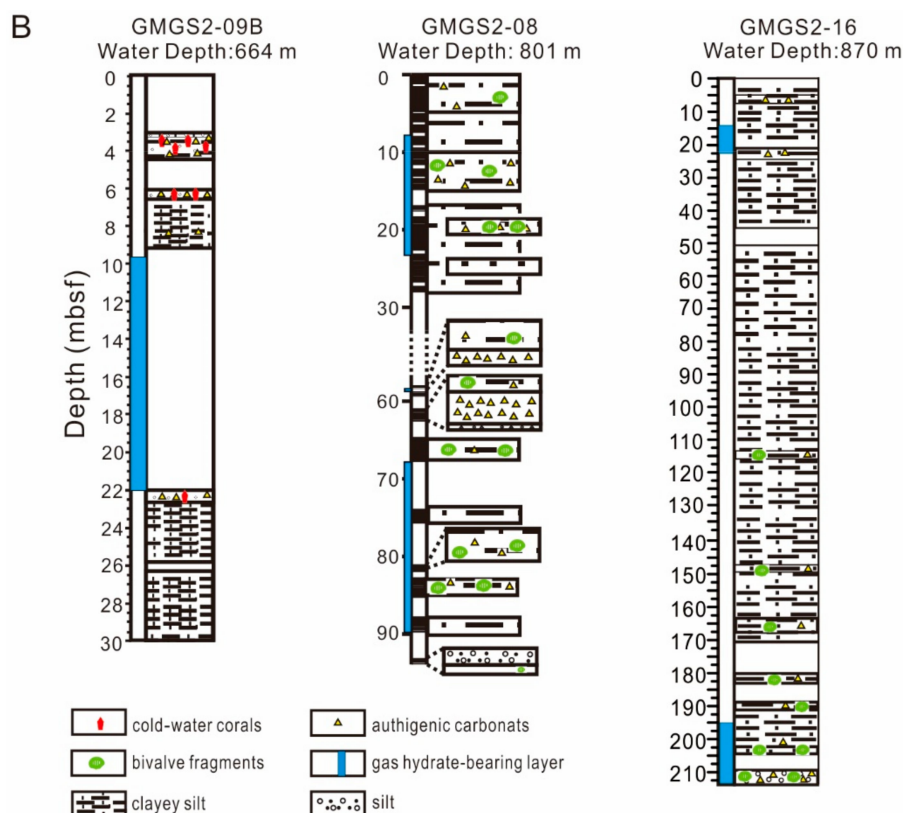


Figure 2. (A) Seismic images of sites GMGS2-08, GMGS2-09B, and GMGS2-16. The vertical lines indicate position of cores. (B) Distribution of cold-water corals and authigenic carbonates at sites GMGS2-08, GMGS2-09B, and GMGS2-16.

2. Geological Background

The northern SCS is an Atlantic-type passive continental margin, with extensive troughs, seamounts, and basins, including the Xisha Trough, Pearl River Mouth Basin, Beibuwan Basin, Qiongdongnan Basin, and Taixinan Basin [48]. The investigated area is located in the Dongsha area, which is situated in the eastern part of the Pearl River Mouth Basin of the SCS, at a water depth of ~664 m (Figure 1). Faults and mud diapirs, which are considered to be effective pathways for hydrocarbon migration, are common in the area [49]. The depths of bottom simulating reflectors are in the range of 160–220 m below the seafloor (mbsf) with an average depth of 180 mbsf [48]. Active cold-seep authigenic carbonates and benthic seep biota have been observed in the Dongsha area [49–51]. Moreover, gas hydrates have been recovered at this site during GMGS-2 in 2013 [48,52].

Gas hydrates were recovered during the GMGS-2 cruise conducted by the Chinese Geological Survey in coordination with Fugro and Geotek in 2013, with drill cores taken at sites GMGS2-08, GMGS2-09B, and GMGS2-16 (Figure 1). Authigenic carbonate nodules and chemosynthetic bivalve shells are common in the three cores. Three fossil CWC skeleton layers were identified in GMGS2-09B core samples, at depths of 3.00–4.47, 6.00–6.42, and 22.00–22.60 mbsf (Figure 2).

3. Samples and Methods

3.1. Samples

Drill core samples were collected at site GMGS2-09B. Gas hydrates containing >99% methane were recovered at depths ranging from 9 to 21 mbsf (Figure 2). There is an extraordinarily high sedimentation rate of ~73.3 cm/k.y. since 0.12 Ma at GMGS2-09B [48]. These samples exhibit both nodular and massive morphologies. The drilling depth reached ~105 mbsf in a water depth of 664 m. The dominant sediments were clayey silt and silt. Samples of fossil CWCs and authigenic carbonate

nodules were obtained. The AMS¹⁴C (¹⁴C accelerator mass spectrometry) ages cluster of the CWCs obtained at 3.35–3.55 mbsf between 15.1 and 15.5 ka BP, and CWCs at 6.20–6.30 mbsf have an age of 17.1 ka BP (unpublished data). All samples were washed immediately after collection and placed in storage at 4 °C.

3.2. Analytical Methods

Well-preserved (without apparently crushed) fossil CWCs and authigenic carbonate samples were selected and further cleaned with deionized water using an ultrasonic cleaner in the laboratory. The shell fragments were separated from adhered sediments under a microscope to remove possible contaminants. CWCs were investigated using Stereo microscope (Discovery V20) and 3D X-ray microscope using an Xradia520 Versa instrument (Zeiss, Oberkochen, Germany) at the Guangzhou Marine Geological Survey and at Carl Zeiss, Shanghai Co., Ltd. (Shanghai, China), respectively. Subsamples from aragonite skeletons of CWCs were collected for geochemical analyses, and all samples were crushed and pulverized to pass through a 200 mesh.

X-ray Powder Diffraction analysis (XRD) was used for semi-quantitative characterizations of CWC mineralogy using a Rigaku D/MAX 2500PC Diffractometer (Tokyo, Japan) equipped with a diffracted beam graphite monochromator and using Cu K α radiation at the Guangzhou Marine Geological Survey. Scans were conducted from 2.5° to 65° (2 θ) at 0.01°/s, using a 300 mA current and 40 kV acceleration voltage. The relative proportions of carbonate minerals were quantified by whole pattern fitting and Rietveld refinement of the MDI Jade 6 program (V6.1, MDI, CA, United States).

Carbon and oxygen isotope values of CWCs and authigenic carbonates were analyzed at the Guangzhou Marine Geological Survey laboratory, following the procedure described by Chen et al. [53]. Samples were processed with 100% phosphoric acid at 80 °C to release CO₂ for measurement using a Kiel IV online carbonate preparation line connected to a MAT 253 mass spectrometer (Thermo Scientific, Waltham, MA, United States). The isotope values are expressed using δ notation relative to the Vienna Pee Dee Belemnite (VPDB) standard. Precisions based on repeated measurements of carbonate standards are in the order of 0.1‰ (2 σ) for both $\delta^{13}\text{C}$ and $\delta^{18}\text{O}$.

Major- and trace-element analysis was performed with HF–HNO₃ solutions following the procedure established by Hu et al. [54]. Major elements were analyzed via inductively coupled plasma–optical emission spectrometry (ICP–OES) (Optima 8300, PerkinElmer, Waltham, MA, United States) and trace elements were measured via ICP–mass spectrometry (MS) (X Series2, Thermo Fisher Scientific, Waltham, MA, United States) at the Guangzhou Marine Geological Survey. The analytical precision of element contents is better than 5%.

4. Results

4.1. Distribution and Species of CWCs

The abundance of CWCs decreases with depth, with distinct layers of higher abundance at 3.00–4.47, 6.00–6.42, and 22.00–22.60 mbsf (Figure 3). Most of the CWCs are fragments 0.063–5 cm in length. The coral fragments' preservation, based on integrity of skeletal structure, ranges from poor to moderate throughout the core. Three genera and two unknown genera were identified, including the solitary corals *Crispatotrochus* sp., *Solenosmilia* sp., and *Enallopsammia* sp. (Figure 4). The most commonly observed CWC fragments were classified as *Solenosmilia* sp. Authigenic carbonates, mainly occurring as gray to gray-white nodules, are found in association with these CWC fragments. These carbonates display a brecciform structure and have lengths of ~0.2–1 cm.

On the basis of microstructures revealed by stereo microscope and micro-CT, three coral species were identified: including *Crispatotrochus* sp., *Solenosmilia* sp., and *Enallopsammia* sp. (Figure 4).

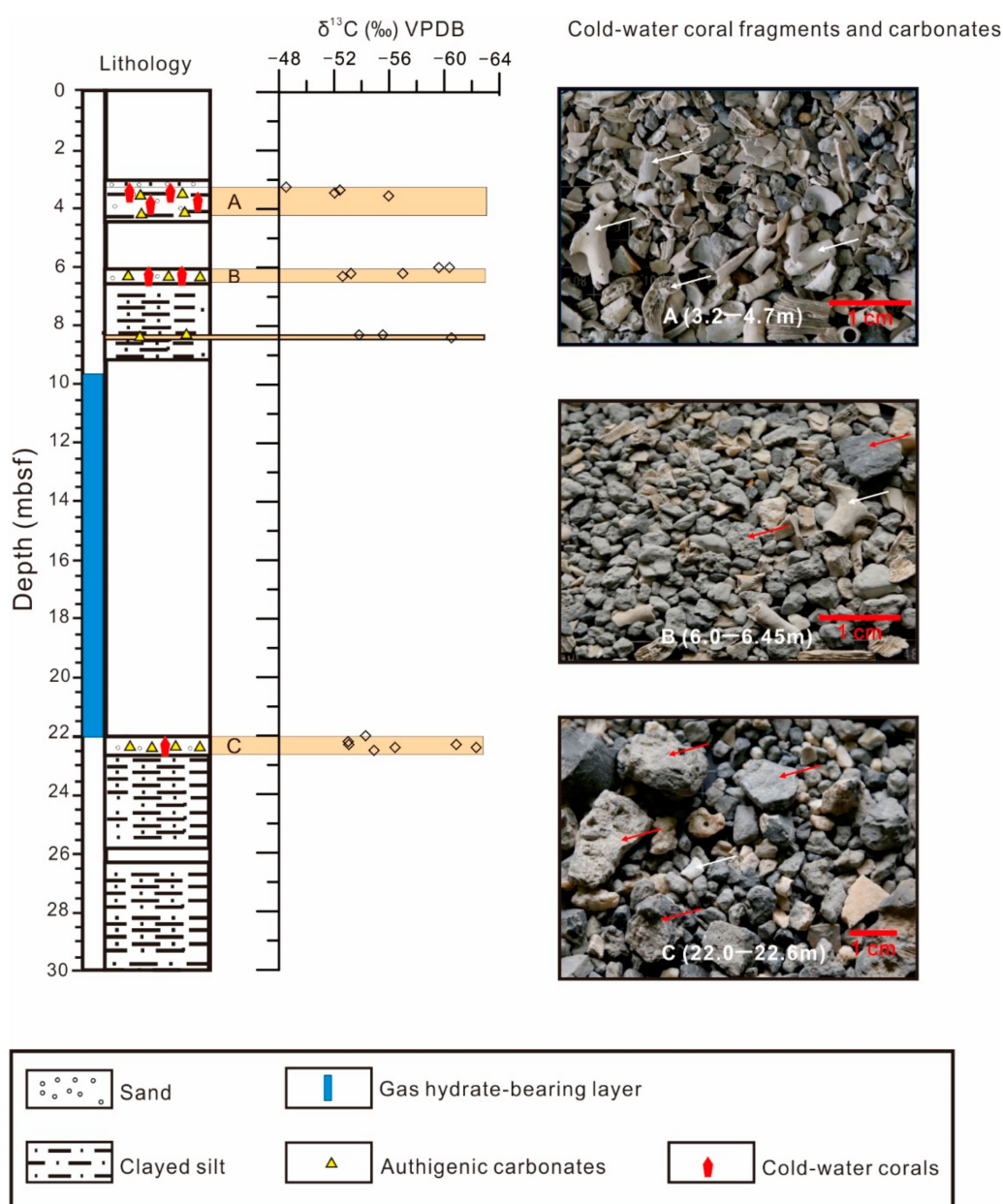


Figure 3. Distribution of cold-water corals and stable isotopes of authigenic carbonates from site GMGS2-09B. The inset images (A–C) are coarse fragments of bulk sediments (>0.063 mm). The white arrows indicate cold-water corals and red arrow indicates the authigenic carbonates.

Crispatotrochus Tenison-Woods, 1878

This genus is a sessile ceratoid solitary coral, with prominent costae, no paliform lobe, and bunchy columella, and does not have a symbiotic relationship with zooxanthellae. The species distribution is Pleistocene to present. Samples: GMGS2-09B at 3.45–3.55 mbsf, incomplete (Figure 4A,B).

Solenosmilia Duncan, 1873

This species exhibits dendritic or bush-shaped complexes, thin walls, and several septa with three complete rounds, or four or five incomplete rounds. The septa of the first and second rounds are long and twisted, with a central connection. Columella are spongy or unapparent. This species does not have a symbiotic relationship with zooxanthellae. Samples: GMGS2-09B at 3.45–3.55 mbsf (Figure 4C,F).

Enallopsammia Michelotti in Sismonda, 1871

This species exhibits dendritic complexes and has thin walls covered by costae. The septa are regularly arranged. The columella is mastoid. This species does not have a symbiotic relationship with zooxanthellae. The species distribution is Pleistocene to present. Samples: GMGS2-09B at 6.30–6.45 mbsf (Figure 4G,H), 6.00–6.15 mbsf (Figure 4I,L), and 3.45–3.55 mbsf (Figure 4K,M).

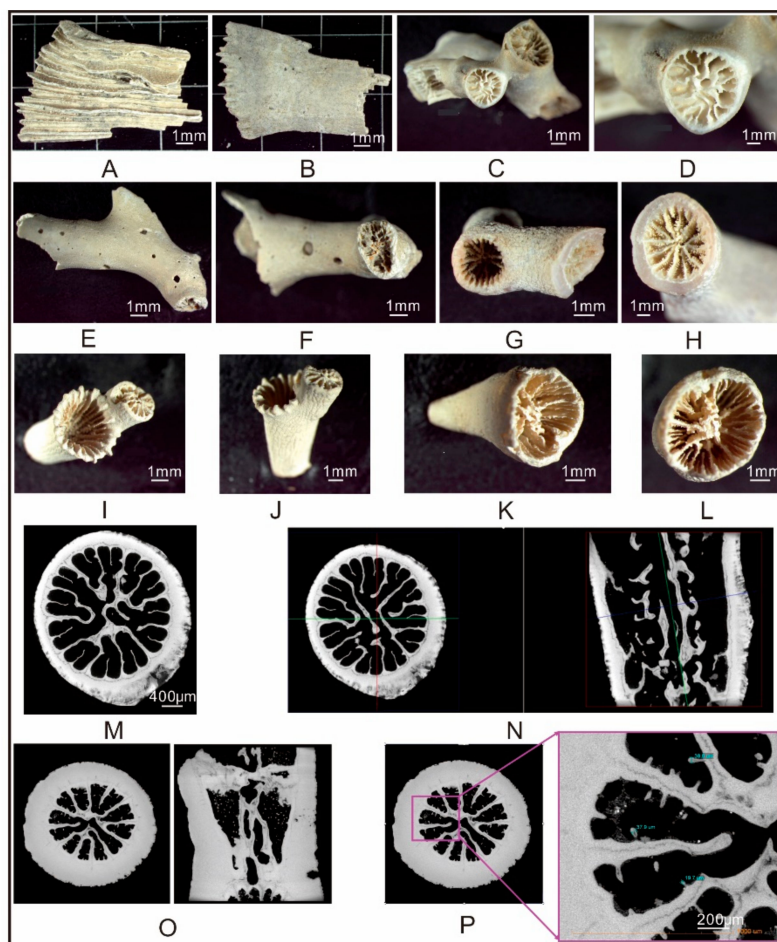


Figure 4. Microscope and micro-CT photos of cold water corals (CWCs) from site GMGS2-09B ((A,B): *Crispatotrochus* sp. Fragment, 345–355 cm; (C–F): *Solenosmilia* sp. 345–355 cm; (G,H): *Enallopsammia* sp., 630–645 cm; (I,J): unknown species A 345–355 cm; (K,L): unknown species B, 600–615 cm; (M,N): *Solenosmilia* sp. cross-sectional view and longitudinal sectional view; (O,P): *Enallopsammia* sp. cross-sectional view and longitudinal sectional view).

4.2. CWC Mineralogy

XRD results show that the CWC samples are 95–99% aragonite, and 1–5% calcite (Table A1), and authigenic carbonate samples are dominated by aragonite, high-Mg calcite, low-Mg calcite and dolomite (unpublished data).

4.3. Carbon and Oxygen Isotopes of CWCs and Carbonates

Stable isotope values for CWCs and carbonates are listed in Table A2 and presented in Figure 5. CWC $\delta^{13}\text{C}$ values range from -8.4‰ to -0.6‰ (mean = -5.3‰ , $n = 48$). The mean $\delta^{13}\text{C}$ values of *Crispatotrochus* sp. and *Solenosmilia* sp. are -6.1‰ and -5.4‰ respectively, but *Enallopsammia* sp. displays a slight ^{13}C enrichment compare to the above corals, with a mean value of -3.8‰ . $\delta^{18}\text{O}$ values for CWCs vary from 0.6‰ to 4.5‰ (mean = 1.9‰ , $n = 48$). *Crispatotrochus* sp. and *Solenosmilia* sp. exhibit similar $\delta^{18}\text{O}$ values that range from 0.6‰ to 3.3‰ (mean = 1.7‰ , $n = 38$). *Enallopsammia* sp. yields higher positive $\delta^{18}\text{O}$ values (mean = 2.5‰ , $n = 7$).

Authigenic carbonates from site GMGS2-09B exhibit extremely negative $\delta^{13}\text{C}$ values ranging from -62.3‰ to -48.5‰ (mean = -55.6‰ , $n = 19$). $\delta^{18}\text{O}$ values range from 3.4‰ to 6.0‰ (mean = 4.4‰ , $n = 19$).

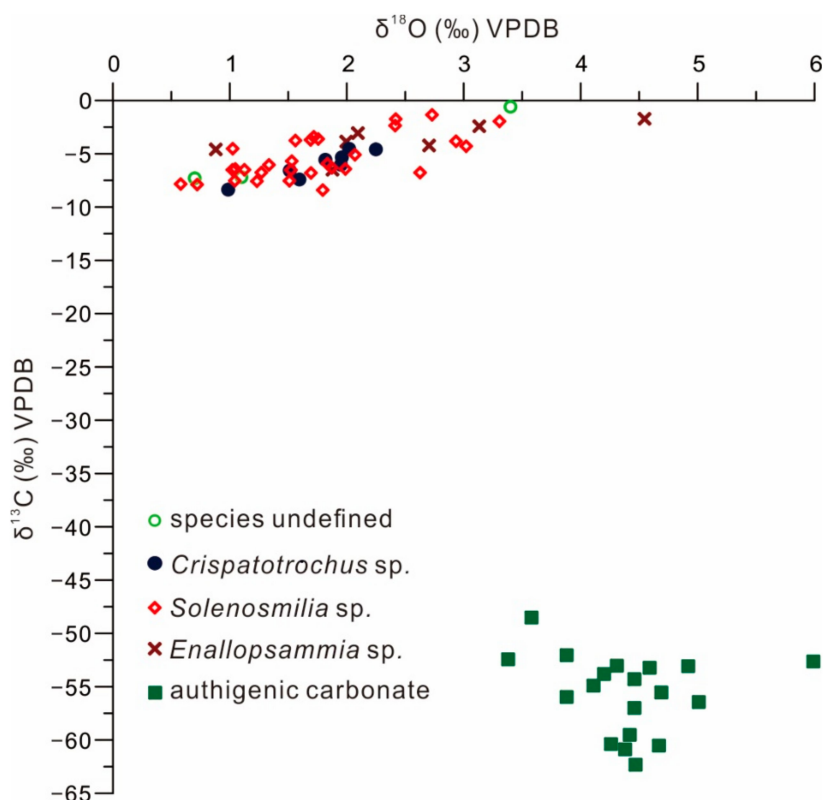


Figure 5. Carbon and oxygen isotopic compositions of CWCs and the associated authigenic carbonates from the South China Sea.

4.4. CWC Element Contents

Contents of major and trace elements in the CWCs are presented in Table A3. Mean calcium contents are 37.89% in *Crispatotrochus* sp., 36.72% in *Solenosmilia* sp., and 38.82% in *Enallopsammia* sp. All samples exhibit similarities in major-element abundances with $\text{Ca} > \text{Na} > \text{K} > \text{Al}$. Contents of Mg, Mn, and Fe are very low, and less than 0.03%.

All samples exhibit similar trace-element contents in the order $\text{Ba} > \text{Ni} > \text{Zn} > \text{U} > \text{Cr} > \text{Cu} > \text{Pb} > \text{Co} > \text{Cd}$ (Table A3). Only Ba, Zn, and Ni show moderate to strong content in the CWC samples, with mean values of 22.36 $\mu\text{g/g}$ for Ba, 9.06 $\mu\text{g/g}$ for Zn, and 10.51 $\mu\text{g/g}$ for Ni. Contents of Cr (2.51–5.25 $\mu\text{g/g}$), Cu (1.30–3.84 $\mu\text{g/g}$), Pb (0.79–3.26 $\mu\text{g/g}$), Co (0.73–1.40 $\mu\text{g/g}$), and Cd (0.082–0.093 $\mu\text{g/g}$) show little variation.

5. Discussion

5.1. CWCs Distribution and Factors Affect Their Growth

The factors determining CWC formation at cold seep areas are largely unknown. Hovland and Thomsen [22] established the “hydraulic theory” on the basis of the presence of cold seeps. These authors posited that hydrocarbon seeps directly fertilize CWCs, a premise supported by the fact that all the studied CWCs are embedded in authigenic carbonates. However, despite the almost identical oceanographic and sedimentological environments of the hydrate drilling area, CWCs were only observed at site GMGS-09B (Figure 2). Even at site GMGS-09B, not all the authigenic carbonate layers contain CWCs. Unlike bivalves and other seep-dwelling animals that directly use

the chemical energy produced by cold-seep processes, CWCs may benefit indirectly from cold seeps through the formation of authigenic carbonates [33]. Authigenic carbonates potentially create a hard substrate for CWC larvae settlement [41]. Although cold-seep activity was widely observed in the research area, observations made by a remotely operated vehicle revealed that authigenic carbonates occurred in seabed only at site GMGS2-09B.

Oceanographic processes have also been regarded as an important factor in CWC development [33,55,56]. Bathymetric highs form areas where eddy currents and internal waves result in increased concentrations of nutrients and a higher food flux for CWCs [56,57]. The shallowest bathymetry recorded during the GMGS-2 survey occurred at site GMGS2-09B (water depth of ~664 m; Figure 2), and the raised seafloor might have resulted in an increased nutrient supply to drive CWC growth [55].

Additional environmental factors favoring CWC growth at site GMGS2-09B are oceanic temperatures and the prevailing hydrodynamic regime [56]. The bottom seawater temperature at site GMGS2-09B was measured as 5.35 °C, which is within the preferred temperature range of 4–13 °C reported for CWCs along continental margins worldwide [1]. In addition, the research area is located in an area where deep Pacific water flows through the Luzon Strait to enter the SCS [47]. This presence of a strong and deep seawater flow should deliver increased nutrients that drive CWC growth. Furthermore, the strong bottom current and the steep and hard seafloor structure prevent deposition of large amounts of debris that could bury CWCs. These favorable oceanographic conditions are likely a significant factor favoring the growth of CWCs in the study area.

5.2. Bottom-Water Chemistry and Fluid Seepage Archived in CWCs

5.2.1. Comparison of C and O Isotope Signatures

As CWCs use HCO_3^- from both ambient seawater and internally produced carbon dioxide for skeleton biomineralization, $\delta^{13}\text{C}$ signatures of coral skeletons can be used to trace external carbon sources [33,58,59]. Food sources will also affect CWC stable isotope values [60]. CWCs may capture live zooplankton or detrital particulate organic matter from the upper water column [1]. Alternatively, it is also possible that they feed on bacterial mats or microorganisms associated with methane fluids [6]. Cold seeps are characterized by widespread chemosynthesis-based ecosystems and are commonly associated with high biomass, fueled by microbial chemosynthesis [61].

However, the data from 48 CWC samples in this study show a linear trend, with obviously high $\delta^{13}\text{C}$ values (−8.4‰ to −0.6‰; Figure 5) compared to those of authigenic carbonates. These values are significantly different from those of the co-occurring authigenic carbonates. The highly ^{13}C -depleted authigenic carbonates (mean = −55.6‰, $n = 19$) at the four intervals (3.25–3.65, 6–6.45, 8.30–8.45, and 22–22.6 mbsf) in core GMGS2-09B indicate a methane-derived isotopic signature, indicating the presence of past methane seepages at the times of deposition of these intervals (Figure 5). Biogenic methane typically exhibits $\delta^{13}\text{C}$ values in the range of −110‰ to −50‰ [62] and thermogenic methane in the range of −50‰ to −30‰ [63]. The extremely negative $\delta^{13}\text{C}$ values of the carbonates (−62.3‰ to −48.5‰) from core GMGS2-09B indicate that the dominant source of carbon fueling the system is biogenic methane.

A summary of $\delta^{13}\text{C}$ and $\delta^{18}\text{O}$ values of CWCs, coral reefs, and carbonates in the SCS and other locations are shown in Figure 6. The values exhibited by the CWCs and carbonates of the present study differ markedly from those from shallow coral reefs at the Xisha Islands [64] and Sanya Bay [65] in the SCS. Carbonates from hydrothermal sites from Mariana Forearc [66] and Lost City [67] show higher $\delta^{13}\text{C}$ values relative to the authigenic carbonates and CWCs from site GMGS2-09B, indicating that the research area is not influenced by low-temperature hydrothermal processes. Our data are comparable with the ranges of $\delta^{13}\text{C}$ and $\delta^{18}\text{O}$ values in CWCs from the North Atlantic [68] and the Japan Sea [69], particularly those from the Dongsha area in the SCS [70,71], which does not have any cold-seep activity. As such, our results do not support the idea that CWCs take up methane-derived carbon at fluid-seepage

areas. We therefore postulate that the primary food sources for CWCs are phytoplankton, zooplankton, and dissolved organic matter, as proposed by other studies [26,72]. However, more work on living coral skeletons is needed to verify this conclusion.

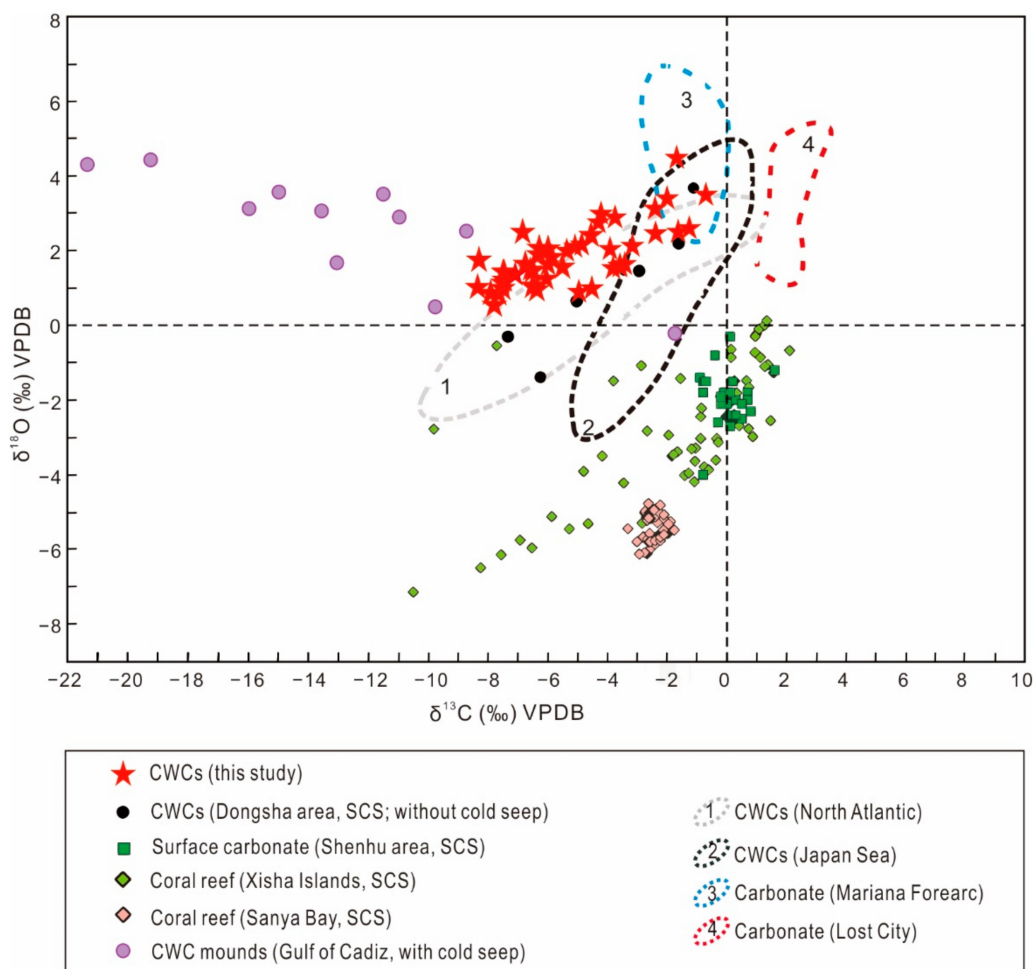


Figure 6. A comparison of carbon and oxygen isotopic compositions of CWCs from the South China Sea and other regions. Data from Pirlet et al. [30], Zhang and He. [64], Ke et al. [65], Tran et al. [66], Früh-Green et al. [67], Blamart et al. [68], Shirai et al. [69], and Chen et al. [70].

The strong linear trend of $\delta^{18}\text{O}$ and $\delta^{13}\text{C}$ from CWCs may be exploited for reconstructing temperature of past climates [1]. However, $\delta^{18}\text{O}$ appear to have a relatively weak covariance with respect to $\delta^{13}\text{C}$ in this study (Figure 6). The most reasonable explanation is that this observation is a result of gas hydrate dissociation. Decomposition of gas hydrate could liberate ^{18}O -rich water with methane [35,50,53]. During an intense methane seepage, this fluid is transported from the sedimentary subsurface to the seabed and into the water column, resulting in alteration of $\delta^{18}\text{O}$ in porewater and bottom seawater [51,54]. This environment would favor heavier $\delta^{18}\text{O}$ values of CWCs during skeleton precipitation. The variance of oxygen isotopes in CWCs caused by gas hydrate dynamics is also supported by occurrence of gas hydrate resources at depth of 9–21 mbsf in GMGS2-09B (Figure 2).

5.2.2. CWC Trace-Element Contents

Trace-element contents in skeletal corals have been used to reconstruct oceanographic conditions [73], but there is very limited information on baseline levels of trace elements in CWCs [7], particularly in cold-seep areas. This study provides the first reported trace-element contents in the fossil CWCs *Crispatotrochus* sp., *Enallopsammia* sp., and *Solenosmilia* sp., collected at SCS cold seeps.

Metal contents within CWC skeletons are controlled by two main factors: the external environment and vital effects [74]. It is considered that the uptake and accumulation of elements in corals during metabolic and physiological processes are influenced by the ambient environmental conditions, including organic matter availability, salinity, production cycle, and seawater temperature [75]. Trace element contents in CWCs that live in non-seep settings tend to be fairly low under the conditions of their typical habitat without an additional source of metal elements [7,76].

In general, contents of Cr, Co, Ni, Cu, Zn, Cd, Pb, U, Ba, Th, and Sr in the samples from core GMGS2-09B are similar to or higher than those observed in modern CWCs from non-seep marine environments (Figure 7). Crocket et al. [77] suggested that such high trace-element contents could be derived from contaminant phases. However, the absence of a systematic relationship between Fe, Mn, Al, and other trace elements (Figure S1) indicates that ambient contamination is not likely the primary influence on CWC trace-element contents. High metal contents are presumably related to the existence of an additional source of trace elements. The contents of Ni and Pb are in good agreement with those found at a hydrothermal site (Azores Islands) (Figure 7), supporting this interpretation. The fluids found in cold seeps contain high concentrations of dissolved trace elements (e.g., Ba), resulting in elemental enrichments in bottom seawater and surface sediments [78,79]. However, the presence of free H₂S produced by intense AOM tends to scavenge trace elements from ambient porewater or seawater, causing subsequent enrichment of redox-sensitive elements (e.g., U and Mo) at cold seeps [53,80]. This is further supported by the obvious enrichment of trace elements (e.g., Mo, U, Pb, Zn and Cu) in seep-impacted aragonites that forming close to the sediment-water interface with free H₂S in sediment pore water [81]. Our results suggest that CWCs might record the influence of biogeochemical processes of fluid seepage on bottom water chemistry.

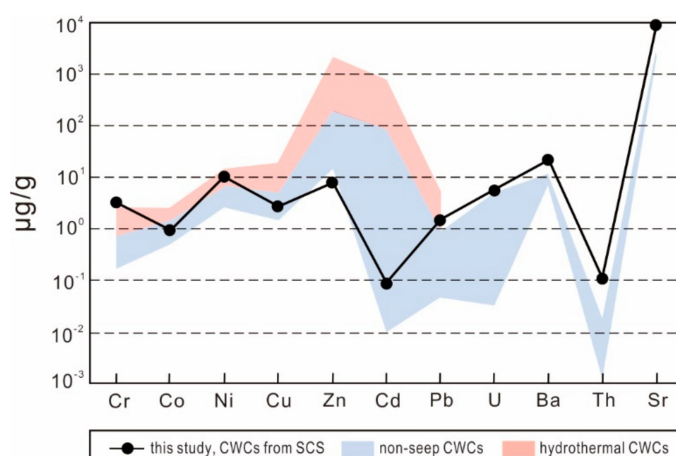


Figure 7. Trace-element contents of CWCs from site GMGS2-09B. Published data from modern CWCs [2,7,76,77] and CWCs in a hydrothermal site [7] are included for comparison.

The geochemical and isotopic signatures and mineralogy of authigenic carbonates are widely used to trace the composition of ascending fluids, seepage intensities, and associated environmental parameters [78,82–85]. The CWCs in seep environments can record rapid changes in ocean chemistry, providing an important constraint on bottom water environmental conditions [26]. As such, the combined study of authigenic carbonates and associated CWCs in seep environments is potentially useful to calibrate the geochemical signatures within authigenic carbonates to aid in reconstruction of past conditions (Figure 8). In addition, U–Th dating of authigenic carbonates is a powerful tool that can also contribute to our understanding of the geological factors and processes controlling seabed methane release [86–91]. However, accurate dating of authigenic carbonates is difficult owing to contamination by detrital terrestrial material [84]. Furthermore, CWC geochronology can potentially provide information about the cessation of cold seep activity, as CWCs use authigenic carbonates as a substrate for colonization.

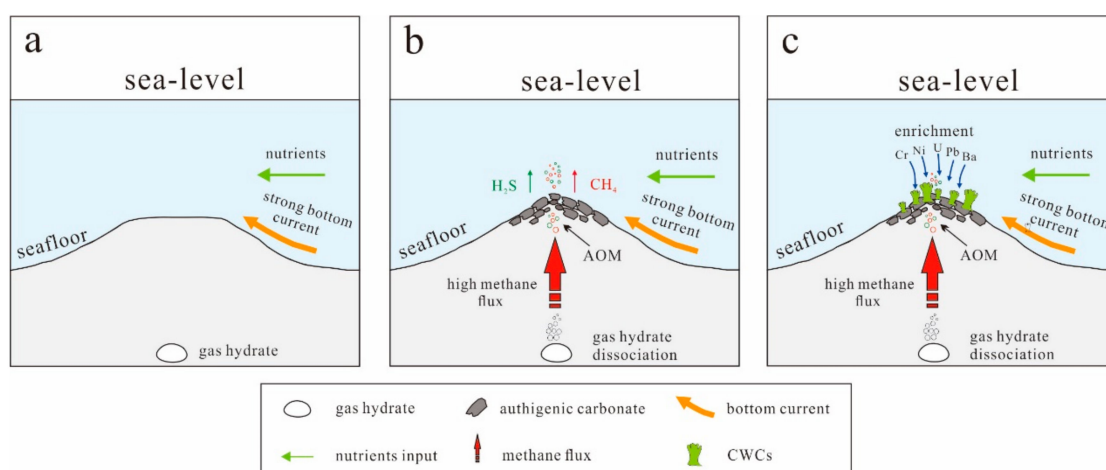


Figure 8. A schematic growth model of formation of CWCs in cold seep area. (a) The absence of cold seep activities in the marine environment. (b) Extensive authigenic carbonates are precipitated close to the sediment-water interface during anaerobic oxidation of methane (AOM) due to enhanced fluid flow associated with dissociation of gas hydrate, providing hard substrates on the seafloor. (c) CWCs settle on the hard carbonate substrates and then are sustained by bottom current and nutrient input. Trace elements may be enriched in CWCs skeleton based on the presence of free H_2S produced by intense AOM.

6. Conclusions

A combined study of three gas-hydrate-bearing sediment cores in the SCS reveal that CWCs were only found at one core and embedded with authigenic carbonates. The close relationship between CWCs and authigenic carbonates is due to the CWCs using authigenic carbonates as a substratum for colonization. Stable isotope studies suggest the source of carbon for CWCs is not directly from fluid seepage. It is suggested that the development of CWCs also require a high seabed topography, appropriate water temperature and stronger bottom-water current. However, in the case of strong fluid seepage, a large amount of nutrient elements will release into the bottom water. This information will be recorded by the coral skeletons. Therefore, CWCs from cold seep area could record the period of the latest cold seep activity, and the detailed geochemical study of CWCs will reveal environmental information during their growth period.

Supplementary Materials: The following are available online at <http://www.mdpi.com/2075-163X/9/12/742/s1>, Figure S1: The relationship between Fe, Al, U, Cr and Cd of cold-water coral samples from the South China Sea.

Author Contributions: Methodology, Y.D. and M.J.; data curation, J.C., H.C., Y.Z., C.W., C.Z., Y.Z. and S.C.; writing—original draft preparation, Y.D.; writing—review and editing, F.C. and N.L.; supervision, F.C.; project administration, F.C.; funding acquisition, F.C. and N.L.

Funding: This research was financial supported by the National Natural Science Foundation of China (Grants: 41776066, 41706053, 41803026 and 41976061), Key Special Project for Introduced Talents Team of Southern Marine Science and Engineering Guangdong Laboratory (Guangzhou) (GML2019ZD0506), Yunnan University's Research Innovation Fund for Graduate Students (2019z046), the China Ocean Mineral Resources R&D Association (Program: DY135-C1-1-04), and Key Laboratory of Marine Mineral Resources, Ministry of Natural Resources (No. KLMMR-2015-A-03).

Acknowledgments: Thanks to the crew and scientists of the GMGS-2 gas hydrate drilling expedition. We deeply appreciate Meixia Zhao (SCSIO, CAS) for identification and Longan Jiao (Carl Zeiss, Shanghai Co., Ltd.) for CT scans of the CWCs.

Conflicts of Interest: The authors declare no conflict of interest.

Appendix A

Table A1. Mineral compositions of cold-water coral fragments from the South China Sea.

Depth (cmbsf)	Sample	Ara	Cal
335–345	<i>Cri.</i>	99	1
345–355	<i>Cri.</i>	97	3
345–355	<i>Sol.</i>	99	1
345–355	<i>Sol.</i>	95	5
345–355	<i>Sol.</i>	98	2
355–365	<i>Sol.</i>	99	1
355–365	<i>Ena.</i>	97	3
630–645	<i>Ena.</i>	99	1

Note: *Cri.*—*Crispatotrochus* species; *Sol.*—*Solenosmilia* species; *Ena.*—*Enallopsammia* species; Ara—aragonite; Cal—calcite.; cmbsf—cm below seafloor.

Table A2. Stable carbon and oxygen isotopes of cold-water corals and associated authigenic carbonates from the gas hydrate-bearing sediments of the South China Sea.

Core Number	Depth (cmbsf)	Sample Type	$\delta^{13}\text{C}$ (‰)	$\delta^{18}\text{O}$ (‰)
09B-2M-1a	325–335	Grey nodular carbonate	−48.5	3.6
09B-2M-1a	335–345	Grey nodular carbonate	−52.4	3.4
09B-2M-1a	345–355	Grey nodular carbonate	−52.0	3.9
09B-2M-1a	355–365	Grey nodular carbonate	−56.0	3.9
09B-2M-1a	600–615	Grey nodular carbonate	−59.5	4.4
09B-2M-1a	620–630	Grey nodular carbonate	−57.0	4.5
09B-2M-1a	620–630	Opalescent nodular carbonate	−53.2	4.6
09B-2M-1a	630–645	Grey nodular carbonate	−52.6	6.0
09B-2M-1a	630–645	Opalescent nodular carbonate	−60.4	4.3
09B-2M-1a	830–840	Opalescent nodular carbonate	−53.8	4.2
09B-2M-1a	830–840	Grey nodular carbonate	−55.5	4.7
09B-2M-1a	840–845	Grey nodular carbonate	−60.5	4.7
09B-5H-1	2200–2215	Grey nodular carbonate	−54.3	4.5
09B-5H-1	2220–2230	Grey nodular carbonate	−53.0	4.3
09B-5H-1	2230–2240	Opalescent nodular carbonate	−60.9	4.4
09B-5H-1	2230–2240	Grey nodular carbonate	−53.1	4.9
09B-5H-1	2240–2250	Opalescent nodular carbonate	−62.3	4.5
09B-5H-1	2240–2250	Grey nodular carbonate	−56.4	5.0
09B-5H-1	2250–2260	Grey nodular carbonate	−54.9	4.1
09B-2M-1a	325–335	<i>Crispatotrochus</i> species	−5.6	1.8
09B-2M-1a	325–335	<i>Crispatotrochus</i> species	−7.4	1.6
09B-2M-1a	325–335	<i>Crispatotrochus</i> species	−5.3	2.0
09B-2M-1a	335–345	<i>Crispatotrochus</i> species	−6.6	1.5
09B-2M-1a	335–345	<i>Crispatotrochus</i> species	−8.4	1.0
09B-3M-1	630–645	<i>Crispatotrochus</i> species	−4.6	2.2
09B-5H-1	2230–2240	<i>Crispatotrochus</i> species	−6.0	2.0
09B-2M-1a	345–355	<i>Crispatotrochus</i> species	−4.5	2.0
09B-5H-1	2200–2215	<i>Enallopsammia</i> species	−3.1	2.1
09B-5H-1	2200–2215	<i>Enallopsammia</i> species	−6.5	1.9
09B-5H-1	2230–2240	<i>Enallopsammia</i> species	−3.9	2.0
09B-5H-1	2220–2230	<i>Enallopsammia</i> species	−4.2	2.7
09B-3M-1	630–645	<i>Enallopsammia</i> species	−2.4	3.1
09B-3M-1	630–645	<i>Enallopsammia</i> species	−1.7	4.5
09B-2M-1a	2220–2230	<i>Enallopsammia</i> species	−4.6	0.9
09B-2M-1a	335–345	<i>Solenosmilia</i> species	−1.3	2.7
09B-2M-1a	335–345	<i>Solenosmilia</i> species	−4.5	1.0
09B-2M-1a	335–345	<i>Solenosmilia</i> species	−6.5	1.1

Table A2. Cont.

Core Number	Depth (cmbsf)	Sample Type	$\delta^{13}\text{C}$ (‰)	$\delta^{18}\text{O}$ (‰)
09B-2M-1a	335–345	<i>Solenosmilia</i> species	−7.6	1.2
09B-2M-1a	335–345	<i>Solenosmilia</i> species	−7.5	1.5
09B-2M-1a	345–355	<i>Solenosmilia</i> species	−5.9	1.8
09B-2M-1a	345–355	<i>Solenosmilia</i> species	−6.0	1.3
09B-2M-1a	345–355	<i>Solenosmilia</i> species	−6.8	2.6
09B-2M-1a	335–345	<i>Solenosmilia</i> species	−6.4	2.0
09B-2M-1a	345–355	<i>Solenosmilia</i> species	−1.7	2.4
09B-2M-1a	345–355	<i>Solenosmilia</i> species	−3.8	1.6
09B-2M-1a	345–355	<i>Solenosmilia</i> species	−6.3	1.9
09B-2M-1a	345–355	<i>Solenosmilia</i> species	−3.7	1.7
09B-2M-1a	345–355	<i>Solenosmilia</i> species	−6.5	1.5
09B-2M-1a	335–345	<i>Solenosmilia</i> species	−5.1	2.1
09B-2M-1a	345–355	<i>Solenosmilia</i> species	−6.5	1.0
09B-2M-1a	345–355	<i>Solenosmilia</i> species	−8.4	1.8
09B-2M-1a	345–355	<i>Solenosmilia</i> species	−7.9	0.7
09B-2M-1a	355–365	<i>Solenosmilia</i> species	−2.0	3.3
09B-2M-1a	355–365	<i>Solenosmilia</i> species	−7.8	0.6
09B-3M-1	600–615	<i>Solenosmilia</i> species	−3.8	2.9
09B-3M-1	600–615	<i>Solenosmilia</i> species	−3.4	1.7
09B-3M-1	630–645	<i>Solenosmilia</i> species	−2.4	2.4
09B-5H-1	2200–2215	<i>Solenosmilia</i> species	−3.6	1.8
09B-5H-1	2230–2240	<i>Solenosmilia</i> species	−4.3	3.0
09B-5H-1	2230–2240	<i>Solenosmilia</i> species	−6.4	1.0
09B-5H-1	2220–2230	<i>Solenosmilia</i> species	−7.5	1.0
09B-5H-1	2220–2230	<i>Solenosmilia</i> species	−6.8	1.7
09B-2M-2a	345–355	<i>Solenosmilia</i> species	−6.8	1.3
09B-2M-1a	610–615	<i>Solenosmilia</i> species	−5.7	1.5
09B-2M-1a	335–345	coral (species undefined)	−7.2	1.1
09B-2M-1a	345–355	coral (species undefined)	−7.3	0.7
09B-2M-1a	620–630	coral (species undefined)	−0.6	3.4

Table A3. Major and trace elements contents of cold-water corals from the South China Sea.

Depth	(cmbsf)	345–355	345–355	610–615	2220–2230
Al	(%)	0.021	0.028	0.076	0.036
Fe	(%)	0.003	0.011	0.026	0.002
Mn	(%)	0.0003	0.001	0.002	0.006
P	(%)	0.009	0.023	0.012	0.006
Ti	(%)	0.0001	0.0002	0.0003	0.0005
Ca	(%)	37.89	37.09	36.34	38.82
Mg	(%)	bl	bl	0.046	bl
Na	(%)	1.52	1.47	1.22	2.06
K	(%)	0.021	0.045	0.048	0.1
Cr	($\mu\text{g/g}$)	2.5	2.6	2.9	5.3
Co	($\mu\text{g/g}$)	0.7	0.8	0.9	1.4
Ni	($\mu\text{g/g}$)	9.3	10.6	10.2	12.0
Cu	($\mu\text{g/g}$)	1.3	3.1	2.7	3.8
Zn	($\mu\text{g/g}$)	5.0	8.0	7.0	12.3
Cd	($\mu\text{g/g}$)	0.1	0.1	0.1	0.1
Pb	($\mu\text{g/g}$)	0.8	1.0	1.1	3.3
U	($\mu\text{g/g}$)	4.6	4.4	6.9	7.0
Ba	($\mu\text{g/g}$)	16.2	23.4	20.4	29.5
Th	($\mu\text{g/g}$)	0.1	0.1	0.2	0.1
Sr	($\mu\text{g/g}$)	9218.0	9248.0	9706.0	9853.0

Note: bl-Below detection limit.

References

1. Roberts, J.M.; Wheeler, A.J.; Freiwald, A. Reefs of the deep: The biology and geology of cold-water coral ecosystems. *Science* **2006**, *312*, 543–547. [[CrossRef](#)] [[PubMed](#)]
2. Van de Flierdt, T.; Robinson, L.F.; Adkins, J.F. Deep-sea coral aragonite as a recorder for the neodymium isotopic composition of seawater. *Geochim. Cosmochim. Acta* **2010**, *74*, 6014–6032. [[CrossRef](#)]
3. Frank, N.; Paterne, M.; Ayliffe, L.; van Weering, T.; Henriot, J.P.; Blamart, D. Eastern North Atlantic deep-sea corals: Tracing up per intermediate water Delta C-14 during the Holocene. *Earth Planet. Sci. Lett.* **2004**, *219*, 297–309. [[CrossRef](#)]
4. Davies, A.J.; Guinotte, J.M. Global habitat suitability for framework-forming cold-water corals. *PLoS ONE* **2011**, *6*, e18483. [[CrossRef](#)] [[PubMed](#)]
5. Margolin, A.R.; Robinson, L.F.; Burke, A.; Waller, R.G.; Scanlon, K.M.; Roberts, M.L.; Auro, M.E.; Van de Flierdt, T. Temporal and spatial distributions of cold-water corals in the Drake Passage: Insights from the last 35,000 years. *Deep-Sea Res. Part II* **2014**, *99*, 237–248. [[CrossRef](#)]
6. Hovland, M.; Risk, M. Do Norwegian deep-water coral reefs rely on seeping fluids? *Mar. Geol.* **2003**, *198*, 83–96. [[CrossRef](#)]
7. Raimundo, J.; Vale, C.; Caetano, M.; Anes, B.; Carreiro-Silva, M.; Martins, I.; de Matos, V.; Porteiro, F.M. Element concentrations in cold-water gorgonians and black coral from Azores region. *Deep-Sea Res. Part II* **2013**, *98*, 129–136. [[CrossRef](#)]
8. Edwards, R.; Chen, J.H.; Wasserburg, G.J. ^{238}U ^{234}U ^{230}Th ^{232}Th systematics and the precise measurement of time over the past 500,000 years. *Earth Planet. Sci. Lett.* **1987**, *81*, 175–192. [[CrossRef](#)]
9. Mortlock, R.A.; Fairbanks, R.G.; Chiu, T.C.; Rubenstone, J. Th-230/U-234/U-238 and Pa-231/U-235 ages from a single fossil coral fragment by multi-collector magnetic-sector inductively coupled plasma mass spectrometry. *Geochim. Cosmochim. Acta* **2005**, *69*, 649–657. [[CrossRef](#)]
10. Robinson, L.F.; Adkins, J.F.; Fernandez, D.P.; Burnett, D.S.; Wang, S.L.; Gagnon, A.C.; Krakauer, N. Primary U distribution in scleractinian corals and its implications for U series dating. *Geochem. Geophys. Geosy.* **2006**, *7*, Q05022. [[CrossRef](#)]
11. Chen, T.Y.; Robinson, L.F.; Burke, A.; Southon, J.; Spooner, P.; Morris, P.J.; Ng, H.C. Synchronous centennial abrupt events in the ocean and atmosphere during the last deglaciation. *Science* **2015**, *349*, 1537–1541. [[CrossRef](#)] [[PubMed](#)]
12. Chen, T.Y.; Robinson, L.F.; Beasley, M.P.; Claxton, L.M.; Andersen, M.B.; Gregoire, L.J.; Wadham, J.; Fornari, D.J.; Harpp, K.S. Ocean mixing and ice-sheet control of seawater U-234/U-238 during the last deglaciation. *Science* **2016**, *354*, 626–629. [[CrossRef](#)] [[PubMed](#)]
13. Lee, J.M.; Eltgroth, S.F.; Boyle, E.A.; Adkins, J.E. The transfer of bomb radiocarbon and anthropogenic lead to the deep North Atlantic Ocean observed from a deep sea coral. *Earth Planet. Sci. Lett.* **2017**, *458*, 223–232. [[CrossRef](#)]
14. Burke, A.; Robinson, L.F. The Southern Ocean's Role in Carbon Exchange during the Last Deglaciation. *Science* **2012**, *335*, 557–561. [[CrossRef](#)]
15. Hines, S.K.V.; Southon, J.R.; Adkins, J.F. A high-resolution record of Southern Ocean intermediate water radiocarbon over the past 30,000 years. *Earth Planet. Sci. Lett.* **2015**, *432*, 46–58. [[CrossRef](#)]
16. Robinson, L.F.; van de Flierdt, T. Southern Ocean evidence for reduced export of North Atlantic Deep Water during Heinrich event 1. *Geology* **2009**, *37*, 195–198. [[CrossRef](#)]
17. Copard, K.; Colin, C.; Henderson, G.M.; Scholten, J.; Douville, E.; Sicre, M.A.; Frank, N. Late Holocene intermediate water variability in the northeastern Atlantic as recorded by deep-sea corals. *Earth Planet. Sci. Lett.* **2012**, *313*, 34–44. [[CrossRef](#)]
18. Montero-Serrano, J.C.; Frank, N.; Tisnerat-Laborde, N.; Colin, C.; Wu, C.C.; Lin, K.; Shen, C.C.; Copard, K.; Orejas, C.; Gori, A.; et al. Decadal changes in the mid-depth water mass dynamic of the Northeastern Atlantic margin (Bay of Biscay). *Earth Planet. Sci. Lett.* **2013**, *364*, 134–144. [[CrossRef](#)]
19. Mitsuguchi, T.; Matsumoto, E.; Abe, O.; Uchida, T.; Isdale, P.J. Mg/Ca thermometry in coral-skeletons. *Science* **1996**, *274*, 961–963. [[CrossRef](#)]
20. Turley, C.M.; Roberts, J.M.; Guinotte, J.M. Corals in deep-water: Will the unseen hand of ocean acidification destroy cold-water ecosystems? *Coral Reefs* **2007**, *26*, 445–448. [[CrossRef](#)]

21. Tittensor, D.P.; Baco, A.R.; Brewin, P.E.; Clark, M.R.; Consalvey, M.; Hall-Spencer, J.; Rowden, A.A.; Schlacher, T.; Stocks, K.I.; Rogers, A.D. Predicting global habitat suitability for stony corals on seamounts. *J. Biogeogr.* **2009**, *36*, 1111–1128. [[CrossRef](#)]
22. Hovland, M.; Thomsen, E. Cold-water corals—Are they hydrocarbon seep related? *Mar. Geol.* **1997**, *137*, 159–164. [[CrossRef](#)]
23. Naeth, J.; di Primio, R.; Horsfield, B.; Schaefer, R.G.; Shannon, P.M.; Bailey, W.R.; Henriot, J.P. Hydrocarbon seepage and carbonate mound formation: A basin modelling study from the porcupine basin (offshore Ireland). *J. Pet. Geol.* **2005**, *28*, 147–165. [[CrossRef](#)]
24. Hovland, M. *Deep-Water Coral Reefs: Unique Biodiversity Hot-Spots*; Praxis Publishing: Chichester, UK, 2008; p. 278.
25. Lindberg, B.; Berndt, C.; Mienert, J. The Fugløy Reef at 701 N; acoustic signature, geologic, geomorphologic and oceanographic setting. *Int. J. Earth Sci.* **2007**, *96*, 201–213. [[CrossRef](#)]
26. Liebetrau, V.; Eisenhauer, A.; Linke, P. Cold seep carbonates and associated cold-water corals at the Hikurangi Margin, New Zealand: New insights into fluid pathways, growth structures and geochronology. *Mar. Geol.* **2010**, *272*, 307–318. [[CrossRef](#)]
27. Jones, A.T.; Greinert, J.; Bowden, D.A.; Klaucke, I.; Petersen, C.J.; Netzeband, G.L.; Weinrebe, W. Acoustic and visual characterisation of methane-rich seabed seeps at Omakere Ridge on the Hikurangi Margin, New Zealand. *Mar. Geol.* **2010**, *272*, 154–169. [[CrossRef](#)]
28. León, R.; Somoza, L.; Medialdea, T.; González, F.J.; Diaz-del-Río, V.; Fernández-Puga, M.C.; Maestro, A.; Mata, M.P. Sea-floor features related to hydrocarbon seeps in deep water carbonate-mud mounds of the Gulf of Cádiz: From mud flows to carbonate precipitates. *Geo.-Mar. Lett.* **2007**, *27*, 237–247. [[CrossRef](#)]
29. Schroeder, W.W. Observations of *Lophelia pertusa* and the surficial geology at a deep-water site in the northeastern Gulf of Mexico. *Hydrobiologia* **2002**, *471*, 29–33. [[CrossRef](#)]
30. Pirlet, H.; Wehrmann, L.M.; Foubert, A.; Brunner, B.; Blamart, D.; De Mol, L.; Van Rooij, D.; Dewanckele, J.; Cnudde, V.; Swennen, R.; et al. Unique authigenic mineral assemblages reveal different diagenetic histories in two neighbouring cold-water coral mounds on Pen Duick Escarpment, Gulf of Cadiz. *Sedimentology* **2012**, *59*, 578–604. [[CrossRef](#)]
31. Hovland, M.; Mortensen, P.B.; Brattegard, T.; Strass, P.; Rokoengen, K. Ahermatypic coral banks off Mid-Norway: Evidence for a link with seepage of light hydrocarbons. *Palaios* **1998**, *13*, 189–200. [[CrossRef](#)]
32. Hovland, M.; Jensen, S.; Indreiten, T. Unit pockmarks associated with *Lophelia* coral reefs off mid-Norway: More evidence of control by ‘fertilizing’ bottom currents. *Geo.-Mar. Lett.* **2012**, *32*, 545–554. [[CrossRef](#)]
33. Rincon-Tomas, B.; Duda, J.P.; Somoza, L.; Gonzalez, F.J.; Schneider, D.; Medialdea, T.; Santofimia, E.; Lopez-Pamo, E.; Madureira, P.; Hoppert, M.; et al. Cold-water corals and hydrocarbon-rich seepage in Pompeia Province (Gulf of Cadiz)-living on the edge. *Biogeosciences* **2019**, *16*, 1607–1627. [[CrossRef](#)]
34. Thiel, V.; Peckmann, J.; Seifert, R.; Wehrung, P.; Reitner, J.; Michaelis, W. Highly isotopically depleted isoprenoids: Molecular markers for ancient methane venting. *Geochim. Cosmochim. Acta* **1999**, *63*, 3959–3966. [[CrossRef](#)]
35. Boetius, A.; Ravensschlag, K.; Schubert, C.J.; Rickert, D.; Widdel, F.; Gieseke, A.; Amann, R.; Jorgensen, B.B.; Witte, U.; Pfannkuche, O. A marine microbial consortium apparently mediating anaerobic oxidation of methane. *Nature* **2000**, *407*, 623–626. [[CrossRef](#)] [[PubMed](#)]
36. Peckmann, J.; Gischler, E.; Oschmann, W.; Reitner, J. An early carboniferous seep community and hydrocarbon-derived carbonates from the Harz mountains, Germany. *Geology* **2001**, *29*, 471. [[CrossRef](#)]
37. Peckmann, J.; Thiel, V. Carbon cycling at ancient methane-seeps. *Chem. Geol.* **2004**, *205*, 443–467. [[CrossRef](#)]
38. Reeburgh, W.S. Oceanic methane biogeochemistry. *Chem. Rev.* **2007**, *107*, 486–513. [[CrossRef](#)]
39. Feng, D.; Lin, Z.J.; Bian, Y.Y.; Chen, D.F.; Peckmann, J.; Bohrmann, G.; Roberts, H.H. Rare earth elements of seep carbonates: Indication for redox variations and microbiological processes at modern seep sites. *J. Asian Earth Sci.* **2013**, *65*, 27–33. [[CrossRef](#)]
40. Van Rooij, D.; Blamart, D.; De Mol, L.; Mienis, F.; Pirlet, H.; Wehrmann, L.M.; Barbieri, R.; Maignien, L.; Templer, S.P.; de Haas, H.; et al. Cold-water coral mounds on the Pen Duick Escarpment, Gulf of Cadiz: The MICROSISTEMS project approach. *Mar. Geol.* **2011**, *282*, 102–117. [[CrossRef](#)]
41. Magalhaes, V.H.; Pinheiro, L.M.; Ivanov, M.K.; Kozlova, E.; Blinova, V.; Kolganova, J.; Vasconcelos, C.; McKenzie, J.A.; Bernasconi, S.M.; Kopf, A.J.; et al. Formation processes of methane-derived authigenic carbonates from the Gulf of Cadiz. *Sediment. Geol.* **2012**, *243*, 155–168. [[CrossRef](#)]

42. Le Bris, N.; Arnaud-Haond, S.; Beaulieu, S.; Cordes, E.E.; Hilario, A.; Rogers, A.; van de Gaever, S.; Watanabe, H. Hydrothermal Vents and Cold Seeps. In *The First Global Integrated Marine Assessment, United Nations*; Cambridge University Press: Cambridge, UK, 2016.
43. Vadorpe, T.; Martins, I.; Vitorino, J.; Hebbeln, D.; Garcia, M.; Van Rooij, D. Bottom currents and their influence on the sedimentation pattern in the El Arraiche mud volcano province, southern Gulf of Cadiz. *Mar. Geol.* **2016**, *378*, 114–126. [[CrossRef](#)]
44. Roberts, H.H.; Kohl, B. Temperature control of cold-water coral (*Lophelia*) mound growth by climate-cycle forcing, Northeast Gulf of Mexico. *Deep-Sea Res. Part II* **2018**, *140*, 142–158. [[CrossRef](#)]
45. Bassett-Smith, P.W. XLIII.—Report on the corals from the Tizard and Macclesfield Banks, China Sea. *J. Nat. Hist. Ser.* **1890**, *6*, 353–374. [[CrossRef](#)]
46. Zou, R.L. Studies on the deep water scleractinia from South China Sea—II. Record and narration of species as well as time-spatial distributional characteristics. *Trop. Oceanol.* **1988**, *7*, 74–83. (In Chinese with English Abstract)
47. Liu, Z.F.; Zhao, Y.L.; Colin, C.; Statterger, K.; Wiesner, M.G.; Huh, C.A.; Zhang, Y.W.; Li, X.J.; Sompongchaiyakul, P.; You, C.F.; et al. Source-to-sink transport processes of fluvial sediments in the South China Sea. *Earth-Sci. Rev.* **2016**, *153*, 238–273. [[CrossRef](#)]
48. Zhang, G.X.; Liang, J.Q.; Lu, J.A.; Yang, S.X.; Zhang, M.; Holland, M.; Schultheiss, P.; Su, X.; Sha, Z.B.; Xu, H.N.; et al. Geological features, controlling factors and potential prospects of the gas hydrate occurrence in the east part of the Pearl River Mouth Basin, South China Sea. *Mar. Pet. Geol.* **2015**, *67*, 356–367. [[CrossRef](#)]
49. Suess, E. RV SONNE cruise report SO 177, Sino-German cooperative project, South China Sea Continental Margin: Geological methane budget and environmental effects of methane emissions and gas hydrates. IFM-GEOMAR Reports 2005. Available online: <http://store.pangaea.de/documentation/Reports/SO177.pdf> (accessed on 29 November 2019).
50. Han, X.Q.; Suess, E.; Huang, Y.Y.; Wu, N.Y.; Bohrrmann, G.; Su, X.; Eisenhauer, A.; Rehder, G.; Fang, Y.X. Jiulong methane reef: Microbial mediation of seep carbonates in the South China Sea. *Mar. Geol.* **2008**, *249*, 243–256. [[CrossRef](#)]
51. Feng, D.; Cheng, M.; Kiel, S.; Qiu, J.W.; Yang, Q.H.; Zhou, H.Y.; Peng, Y.B.; Chen, D.F. Using Bathymodiolus tissue stable carbon, nitrogen and sulfur isotopes to infer biogeochemical process at a cold seep in the South China Sea. *Deep-Sea Res. Part II* **2015**, *104*, 52–59. [[CrossRef](#)]
52. Sha, Z.B.; Liang, J.Q.; Zhang, G.X.; Yang, S.X.; Lu, J.G.; Zhang, Z.J.; McConnell, D.R.; Humphrey, G. A seepage gas hydrate system in northern South China Sea: Seismic and well log interpretations. *Mar. Geol.* **2015**, *366*, 69–78. [[CrossRef](#)]
53. Chen, F.; Hu, Y.; Feng, D.; Zhang, X.; Cheng, S.H.; Cao, J.; Lu, H.F.; Chen, D.F. Evidence of intense methane seepages from molybdenum enrichments in gas hydrate-bearing sediments of the northern South China Sea. *Chem. Geol.* **2016**, *443*, 173–181. [[CrossRef](#)]
54. Hu, Y.; Feng, D.; Peckmann, J.; Roberts, H.H.; Chen, D.F. New insights into cerium anomalies and mechanisms of trace metal enrichment in authigenic carbonate from hydrocarbon seeps. *Chem. Geol.* **2014**, *381*, 55–66. [[CrossRef](#)]
55. Foubert, A.; Depreiter, D.; Beck, T.; Maignien, L.; Pannemans, B.; Frank, N.; Blamart, D.; Henriët, J.P. Carbonate mounds in a mud volcano province off north-west Morocco: Key to processes and controls. *Mar. Geol.* **2008**, *248*, 74–96. [[CrossRef](#)]
56. Somoza, L.; Ercilla, G.; Urgorri, V.; Leon, R.; Medialdea, T.; Paredes, M.; Gonzalez, F.J.; Nombela, M.A. Detection and mapping of cold-water coral mounds and living *Lophelia* reefs in the Galicia Bank, Atlantic NW Iberia margin. *Mar. Geol.* **2014**, *349*, 73–90. [[CrossRef](#)]
57. De Mol, B.; Van Rensbergen, P.; Pillen, S.; Van Herreweghe, K.; Van Rooij, D.; McDonnell, A.; Huvenne, V.; Ivanov, M.; Swennen, R.; Henriët, J.P. Large deep-water coral banks in the Porcupine Basin, southwest of Ireland. *Mar. Geol.* **2002**, *188*, 193–231. [[CrossRef](#)]
58. Zoccola, D.; Ganot, P.; Bertucci, A.; Caminiti-Segonds, N.; Techer, N.; Voolstra, C.R.; Aranda, M.; Tambutte, E.; Allemand, D.; Casey, J.R.; et al. Bicarbonate transporters in corals point towards a key step in the evolution of cnidarian calcification. *Sci. Rep.* **2015**, *5*, 9983. [[CrossRef](#)]
59. Nakamura, T.; Nadaoka, K.; Watanabe, A.; Yamamoto, T.; Miyajima, T.; Blanco, A.C. Reef-scale modeling of coral calcification responses to ocean acidification and sea-level rise. *Coral Reefs* **2018**, *37*, 37–53. [[CrossRef](#)]

60. Sherwood, O.A.; Jamieson, R.E.; Edinger, E.N.; Wareham, V.E. Stable C and N isotopic composition of cold-water corals from the Newfoundland and Labrador continental slope: Examination of trophic, depth and spatial effects. *Deep-Sea Res. Part II* **2008**, *55*, 1392–1402. [[CrossRef](#)]
61. Levin, L.A. Ecology of cold seep sediments: Interactions of fauna with flow, chemistry and microbes. *Oceanogr. Mar. Biol.* **2005**, *43*, 1–46.
62. Whiticar, M.J. Carbon and hydrogen isotope systematics of bacterial formation and oxidation of methane. *Chem. Geol.* **1999**, *161*, 291–314. [[CrossRef](#)]
63. Sackett, W.M. Carbon and hydrogen isotope effects during the thermocatalytic production of hydrocarbons in laboratory simulation experiments. *Geochim. Cosmochim. Acta* **1978**, *42*, 571–580. [[CrossRef](#)]
64. Zhang, M.S.; He, Q.X. A study on quaternary stratigraphy of reef deposits on Xisha Islands. *Quat. Sci.* **1989**, *9*, 143–154. (In Chinese with English Abstract)
65. Ke, T.; Wei, G.J.; Liu, Y.; Xie, L.H.; Deng, W.F.; Wang, G.Q.; Xu, J.F. High resolution boron isotopic compositions of a coral from the northern South China Sea and their implications for reconstruction of seawater pH. *Geochimica* **2015**, *44*, 1–8. (In Chinese with English Abstract)
66. Tran, T.H.; Kato, K.; Wada, H.; Fujioka, K.; Matsuzaki, H. Processes involved in calcite and aragonite precipitation during carbonate chimney formation on Conical Seamount, Mariana Forearc: Evidence from geochemistry and carbon, oxygen, and strontium isotopes. *J. Geochem. Explor.* **2014**, *137*, 55–64. [[CrossRef](#)]
67. Fruh-Green, G.L.; Kelley, D.S.; Bernasconi, S.M.; Karson, J.A.; Ludwig, K.A.; Butterfield, D.A.; Boschi, C.; Proskurowski, G. 30,000 years of hydrothermal activity at the Lost City vent field. *Science* **2003**, *301*, 495–498. [[CrossRef](#)]
68. Blamart, D.; Rollion-Bard, C.; Cuif, J.P.; Juillet-Leclerc, A.; Lutringer, A.; van Weering, T.C.E.; Henriot, J.P. C and O Isotopes in A Deep-Sea Coral (*Lophelia Pertusa*) Related to Skeletal Microstructure. In *Cold-Water Corals and Ecosystems*; Freiwald, A., Roberts, J.M., Eds.; Springer: Berlin/Heidelberg, Germany, 2005; pp. 1005–1020.
69. Shirai, K.; Kusakabe, M.; Nakai, S.; Ishii, T.; Watanabe, T.; Hiyagon, H.; Sano, Y. Deep-sea coral geochemistry: Implication for the vital effect. *Chem. Geol.* **2005**, *224*, 212–222. [[CrossRef](#)]
70. Chen, Z.; Mo, A.; Zhao, M.X.; Zhong, Y.; Yan, W. The discovery of deep-water corals from cold seep area in the northern South China Sea and their characteristics. *J. Trop. Oceanogr.* **2018**, *37*, 64–71. (In Chinese with English Abstract)
71. Xu, A.; Chen, Z.; Qu, Y.; Tian, Y.; Shu, C.; Zheng, X.; Li, G.; Yan, W.; Zhao, M. Cold-water corals in a cold seep area on the northern continental slopes of the South China sea and their isotopic characteristics. *Deep-Sea Res. I* **2019**, *153*, 103043. [[CrossRef](#)]
72. Becker, E.L.; Cordes, E.E.; Macko, S.A.; Fisher, C.R. Importance of seep primary production to *Lophelia pertusa* and associated fauna in the Gulf of Mexico. *Deep-Sea Res. Part I* **2009**, *56*, 786–800. [[CrossRef](#)]
73. Fallon, S.J.; White, J.C.; McCulloch, M.T. Porites corals as recorders of mining and environmental impacts: Misima Island, Papua New Guinea. *Geochim. Cosmochim. Acta* **2002**, *66*, 45–62. [[CrossRef](#)]
74. Robinson, L.F.; Adkins, J.F.; Frank, N.; Gagnon, A.C.; Prouty, N.G.; Roark, E.B.; van de Flierdt, T. The geochemistry of deep-sea coral skeletons: A review of vital effects and applications for palaeoceanography. *Deep-Sea Res. Part II* **2014**, *105*, 118. [[CrossRef](#)]
75. Ramos, A.A.; Inoue, Y.; Ohde, S. Metal contents in Porites corals: Anthropogenic input of river run-off into a coral reef from an urbanized area, Okinawa. *Mar. Pollut. Bull.* **2004**, *48*, 281–294. [[CrossRef](#)]
76. Sinclair, D.J.; Williams, B.; Allard, G.; Ghaleb, B.; Fallon, S.; Ross, S.W.; Risk, M. Reproducibility of trace element profiles in a specimen of the deep-water bamboo coral *Keratoisis* sp. *Geochim. Cosmochim. Acta* **2011**, *75*, 5101–5121. [[CrossRef](#)]
77. Crocket, K.C.; Lambelet, M.; de Flierdt, T.V.; Rehkamper, M.; Robinson, L.F. Measurement of fossil deep-sea coral Nd isotopic compositions and concentrations by TIMS as NdO⁺, with evaluation of cleaning protocols. *Chem. Geol.* **2014**, *374*, 128–140. [[CrossRef](#)]
78. Torres, M.E.; McManus, J.; Huh, C.A. Fluid seepage along the San Clemente Fault scarp: Basin-wide impact on barium cycling. *Earth Planet. Sci. Lett.* **2002**, *203*, 181–194. [[CrossRef](#)]
79. Feng, D.; Roberts, H.H. Geochemical characteristics of the barite deposits at cold seeps from the northern Gulf of Mexico continental slope. *Earth Planet. Sci. Lett.* **2011**, *309*, 89–99. [[CrossRef](#)]
80. Hu, Y.; Feng, D.; Liang, Q.Y.; Xia, Z.; Chen, L.Y.; Chen, D.F. Impact of anaerobic oxidation of methane on the geochemical cycle of redox-sensitive elements at cold-seep sites of the northern South China Sea. *Deep-Sea Res. Part II* **2015**, *122*, 84–94. [[CrossRef](#)]

81. Liang, Q.Y.; Hu, Y.; Feng, D.; Peckmann, J.; Chen, L.Y.; Yang, S.X.; Liang, J.Q.; Tao, J.; Chen, D.F. Authigenic carbonates from newly discovered active cold seeps on the northwestern slope of the South China Sea: Constraints on fluid sources, formation environments, and seepage dynamics. *Deep-Sea Res. Part II* **2017**, *124*, 31–41. [[CrossRef](#)]
82. Peckmann, J.; Birgel, D.; Kiel, S. Molecular fossils reveal fluid composition and flow intensity at a Cretaceous seep. *Geology* **2009**, *37*, 847–850. [[CrossRef](#)]
83. Roberts, H.H.; Feng, D.; Joye, S.B. Cold-seep carbonates of the middle and lower continental slope, northern Gulf of Mexico. *Deep-Sea Res. Part II* **2010**, *57*, 2040–2054. [[CrossRef](#)]
84. Bayon, G.; Dupre, S.; Ponzevera, E.; Etoubleau, J.; Cheron, S.; Pierre, C.; Mascle, J.; Boetius, A.; de Lange, G.J. Formation of carbonate chimneys in the Mediterranean Sea linked to deep-water oxygen depletion. *Nat. Geosci.* **2013**, *6*, 755–760. [[CrossRef](#)]
85. Feng, D.; Qiu, J.W.; Hu, Y.; Peckmann, J.; Guan, H.X.; Tong, H.P.; Chen, C.; Chen, J.X.; Gong, S.G.; Li, N.; et al. Cold seep systems in the South China Sea: An overview. *J. Asian Earth Sci.* **2018**, *168*, 3–16. [[CrossRef](#)]
86. Teichert, B.M.A.; Eisenhauer, A.; Bohrmann, G.; Haase-Schramm, A.; Bock, B.; Linke, P. U/Th systematics and ages of authigenic carbonates from Hydrate Ridge, Cascadia Margin: Recorders of fluid flow variations. *Geochim. Cosmochim. Acta* **2003**, *67*, 3845–3857. [[CrossRef](#)]
87. Watanabe, Y.; Nakai, S.; Hiruta, A.; Matsumoto, R.; Yoshida, K. U-Th dating of carbonate nodules from methane seeps off Joetsu, Eastern Margin of Japan Sea. *Earth Planet. Sci. Lett.* **2008**, *272*, 89–96. [[CrossRef](#)]
88. Cremiere, A.; Lepland, A.; Chand, S.; Sahy, D.; Condon, D.J.; Noble, S.R.; Martma, T.; Thorsnes, T.; Sauer, S.; Brunstad, H. Timescales of methane seepage on the Norwegian margin following collapse of the Scandinavian Ice Sheet. *Nat. Commun.* **2016**, *7*, 11509. [[CrossRef](#)]
89. Wu, D.D.; Sun, T.T.; Xie, R.; Pan, M.D.; Chen, X.G.; Ye, Y.; Liu, L.H.; Wu, N.Y. Characteristics of Authigenic Minerals around the Sulfate-Methane Transition Zone in the Methane-Rich Sediments of the Northern South China Sea: Inorganic Geochemical Evidence. *Int. J. Env. Res. Public Health* **2019**, *16*, 2299. [[CrossRef](#)]
90. Xie, R.; Wu, D.D.; Liu, J.; Sun, T.T.; Liu, L.H.; Wu, N.Y. Geochemical Evidence of Metal-Driven Anaerobic Oxidation of Methane in the Shenhu Area, the South China Sea. *Int. J. Env. Res. Public Health* **2019**, *16*, 3559. [[CrossRef](#)]
91. Chen, D.F.; Huang, Y.Y.; Yuan, X.L.; Cathles, L.M. Seep carbonates and preserved methane oxidizing archaea and sulfate reducing bacteria fossils suggest recent gas venting on the seafloor in the northeastern South China Sea. *Mar. Pet. Geol.* **2005**, *22*, 613–621. [[CrossRef](#)]



© 2019 by the authors. Licensee MDPI, Basel, Switzerland. This article is an open access article distributed under the terms and conditions of the Creative Commons Attribution (CC BY) license (<http://creativecommons.org/licenses/by/4.0/>).